ScienceVolks Open Access

SVOA MATERIALS SCIENCE & TECHNOLOGY

(ISSN: 2634-5331)

Research

https://sciencevolks.com/materials-science/

Volume 2 Issue 3

Study on friction and wear behavior of nitrogen expanded martensite under low-load and low-speed sliding condition

Yunxia Chen *

School of Mechanical Engineering, Shanghai Dianji University, Shanghai, 201306, P.R. China

***Corresponding author:** Yunxia Chen, *School of Mechanical Engineering, Shanghai Dianji University, Shanghai, 201306, P.R. China*

Received: *September 08, 2020* ***Published:*** *September 25, 2020*

Abstract:

The friction and wear behavior of nitrogen expanded martensite with different nitrogen contents is analyzed by pin-on-disk tribometer under dry sliding condition. The results show that the friction and wear behavior of nitrogen expanded martensite represents a typical mild-oxidational wear characterized by the generation, compaction and delamination of oxide debris, which is related to the nitrogen content and hardness of expanded martensite. The elevated contact temperature on rubbed surface could vary the kinds of oxides and wear mechanisms.

Keywords: Martensitic steel; Friction; Wear; Nitriding; Expanded martensite

1. Introduction

As similar to S phase (the expanded austenite) [1, 2], the nitrogen expanded martensite α_N phase is defined as the supersaturation solution of nitrogen in martensitic lattice, which is suggested by Kim [3]. The α_N phase is easily obtained by the nitriding of martensitic steels [4-8]. For the conventional nitriding processes (gas or plasma nitriding), the compound layer mainly consisting of nitrides (ε-$Fe_{2-3}N$ and γ-Fe_4N) usually forms on the nitride surface, which represents a good wear resistance with an appropriate proportion of ε-$Fe_{2-3}N$ phase [9-13].

Additionally, Alsaran [14] demonstrated that the nitrided layer without compound layer exhibits a lower wear rate than the case with a thick brittle compound layer, indicating the α_N phase also represents a good wear property. Many factors could affect the wear behavior of materials, such as the surface hardness, microstructures and phase compositions as well as surface roughness [15]. Indeed, the concentration of materials also affects the wear properties by determining the microstructure and forming various oxides debris during the sliding wear [16, 17]. These oxide debris will be compacted to form a wear protective layer called compact particle layer and smooth glaze layer [18], which results in the severe to mild wear transition accompanying with a significant decrease of the friction coefficient and wear rate. Recently, many studies have deeply investigated the effects of nitrided parameters on the wear properties of expanded austenite (S phase) under different sliding wear techniques and environment conditions [19, 20]. However, the friction and wear properties of the α_N phase have not been investigated systematically yet. Results show that the S phase represents an excellent wear resistance without any deterioration of corrosion properties because of its higher hardness, while how about the friction and wear properties of the α_N phase?

In present study, the α_N phase with nitrogen (N) concentration gradient is continuously produced on the M50NiL martensitic steel by plasma nitriding. The friction and wear behaviors of the α_N phase with different N contents are characterized. The purpose of this study is to understand the effect of N content on the friction and wear behavior of the α_N phase.

2. Experimental Procedure

The solution treated (austenitized at 1150°C for 1h then quenched in oil) M50NiL martensitic steel with chemical composition (in wt.%) 0.13C, 4.1Cr, 3.4Ni, 4.2Mo, 1.2V, 0.13Mn, 0.18Si, 0.012P, 0.002S and Fe balance was used. The specimens were cut into the size of 12mm×12mm×4mm and manually ground using SiC papers down to 800 grades to achieve a fine finish. Then the specimens were ultrasonically cleaned with alcohol and acetone before plasma nitriding.

Plasma nitriding were produced in a 30kW plasma nitriding furnace (LDMC-30) which was evacuated to 20 Pa. In order to obtain a single α_N phase, the plasma nitriding was conducted at a constant pressure of 260 Pa in a gas mixture containing N_2 and H_2 with a low ratio of 1:8 at 560℃ for 8h.

The friction and wear behaviors of the αN phase containing various nitrogen contents were evaluated through analyzing the depth-related friction and wear properties. The nitrided layer was removed by step-wise manual grinding and the removed thickness was measured by a spiral micrometer. There were total 12 tested layers including the top surface. All the tested layers were marked as L0-L11 and their depths form surface were listed in Table 1. The friction and wear properties of selected layers were characterized using a pin-on-disc tribometer (POD-1). Dry sliding wear tests were performed against a stationary WC ball of 5mm diameter at the speed 200rpm (0.1m s-1) for 360m and the normal contact load was 5N. All the tests were conducted in air (temperature 20°C, humidity 55%RH). The volume wear rate was calculated according to Eq. (1) [21].

$$\eta = \pi r l^3 / 6RFS \quad \text{.....(1)}$$

Where *r* (mm) is wear track radius, *l* (mm) is wear track width, *R* (mm) is pin ball radius, *F* (N) is normal contact load and *S* (m) is total sliding distance. To make sure of the accuracy of the measured friction coefficients, the same depth layer would be tested for three times.

Table 1. Depth from surface for L0-L11 layers

Layer marks	L0	L1	L2	L3	L4	L5	L6	L7	L8	L9	L10	L11
Distance(m)	0	5	20	35	50	65	80	95	110	120	135	160

The cross-section of plasma nitrided layer and wear morphologies were observed using scanning electron microscope (SEM, FEI QUANTA 200 F). X-ray diffraction (XRD, D/max-rB) with Cu-K radiation (λ-0.15405 nm) was used to obtain the phase composition of each removed layer. The energy dispersive X-ray analyzer (EDS) was used to obtain the N profile of the nitrided layer and to study the wear mechanisms involved. The microhardness profile of the nitrided layer was determined with a microhardness tester (HV-1000) under an indentation load of 100g for 20s. The microhardness and elemental contents would be tested three times to achieve a higher accuracy.

3. Results and Discussions

The cross-sectional morphology and depth-related phase constituents are shown in Figure 1. Figure 1a provides a clear morphology of the nitrided layer consisted of a single α_N phase. The microhardness and N content profiles along depth shown in Figure 1a gradually decrease from the surface to the core with depth increasing, which agrees well with each other. The thickness of the nitrided layer (~110 m) obtained by metallographical method is thinner than that (~150 m) measured by microhardness method, which indicates that there is a diffusion layer (hardness < $800HV_{0.1}$, N content < 1.5wt.%) representing a better corrosion resistance underneath the etched nitrided layer. The difference of etching characterization among each removed layer reflects the difference of oxidation resistance, which probably affects the friction and wear behavior of the corresponding layer, especially oxidation wear.

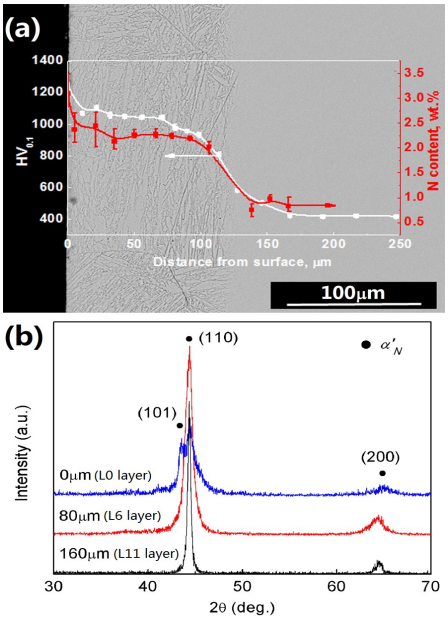

Figure 1. The cross-sectional morphology and depth-related phase constituents

The XRD patterns shown in Figure 1b exhibit a single α_N phase that dominates the whole nitrided layer. For the L0 layer, the main diffraction peak of the α_N phase split into (110) line and (101) line due to the *c*-axis extension of martensite $_{Fe}$ and the difference of interplanar spacing of (101) and (110) planes resulting from the massive incorporation of nitrogen atoms into the martensitic lattice. With the removed depth increasing, the (101) diffraction peak disappears and the peak width of (110) peak becomes narrow, indicating the decrease of N solution.

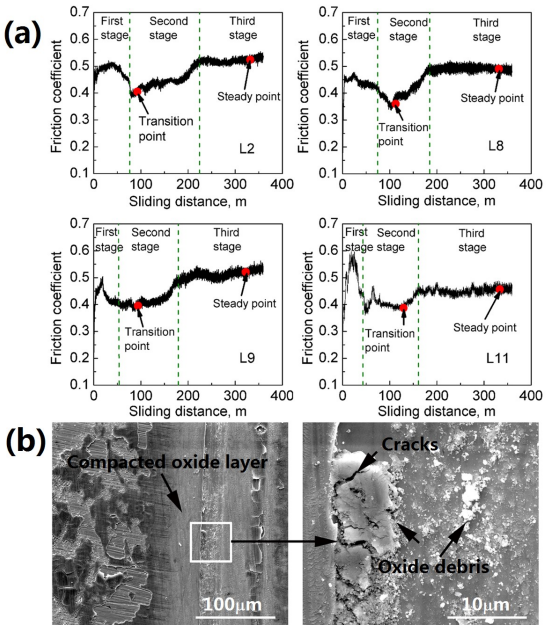

Figure 2. The friction coefficient curves for some removed layers with different microhardness

The transition in friction and wear behavior during sliding wear process could be reflected by the variation of the friction coefficient [22, 23]. Figure 2 gives the typical friction coefficient curves for some removed layers with different microhardness. The variations of friction coefficient are similar in all removed layers investigated in the present study and the processes can be divided into three stages. In the first stage, the friction coefficient increases immediately to a high value of 0.5-0.6 in a short duration due to the initial surface roughness and severe wear of metallic adhesion [22]. Then, in the second stage, the friction coefficient decreases gradually because of the massive oxide debris formation (formed by oxidation of the metallic debris) on the rubbed surface [24]. With the agglomeration and compaction of the wear debris to form a wear-protective layer, the friction coefficient drops to the lowest value of 0.3-0.4 (defined as transition point, see Figure 2a). The duration of the lower level friction coefficient depends on the amount of oxide debris, the stability of the compacted oxide layer and the bearing capacity of the substrate. When the compacted oxide layer reaches its critical thickness, it begins to break off by crack generation, which would enhance the roughness and friction coefficient. Figure 2b represents the cracks initiate and grow at the edge of the compacted layer. The cracked oxide layer is removed completely from the contacting surface, exposing the fresh surface to the environment, which will be reoxidized in the subsequent rubbing. When a dynamic equilibrium process is established, the wear process comes to the third stage, i.e. the friction coefficient remains at a relatively steady value of 0.5-0.6 (defined as steady point, see Figure 2a). The steady wear undergoes an alternating process of oxide debris formation, compaction, and delamination on the rubbed surface [24], which is a typical mild-oxidational wear mode termed an 'oxidation -scrape-reoxidation' mechanism [18].

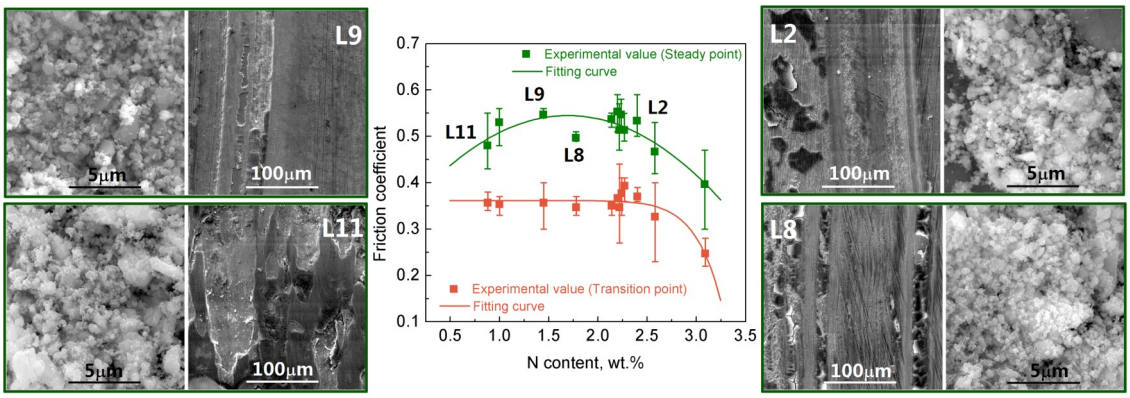

Figure 3. The relationship between the friction coefficient and N content in the *α* N phase

The relationship between the friction coefficient and N content in the αN phase is illustrated in Figure 3 with the wear track and wear debris morphologies of the L2, L8, L9 and L11 layer. It is seen that the friction coefficients of transition points increase with the reduction of N content, reaching a steady value (about 0.35) when the N content decreases to 2.2wt.%. While the variation of friction coefficients of steady points follows an approximate parabolic-law, i.e. the friction coefficient first increases and then decreases with the reduction of N content. It should be noted that the friction coefficient of the steady point for the L8 layer is departed from the parabolic-law, which is lower than the predicted value. Indeed, the variations of friction coefficient depend on the physical and chemical properties of the oxide debris and the bearing capacity of the metal substrate, including the size, amount and kinds of the oxide debris as well as the hardness of the substrate. Stott [25] has demonstrated that only the wear debris with a diameter less than a critical value could stay within the rubbed tracks to form the protective layer against wear damages. Comparing with the morphologies of worn surfaces and wear debris of the L2, L8, L9 and L11 layer, we can find that the L8 layer has the largest fraction of area covered by oxide layer and smallest size of oxide debris, which contributes to its lower friction coefficient. Additionally, the good oxidation resistance of the L8 layer (see Figure 1a) assists in forming a continuous and lubricant oxide film on the contacting surface like stainless steels. The higher friction coefficient for the L2 layer is attributed to the lack of enough oxide debris with small size or probably the higher brittleness of oxide layer caused by the relatively high N content. While the similar friction coefficient for the L9 layer results from the lower bearing capacity of the substrate due to the lower N content and hardness. The L11 layer with lowest hardness represents a lower friction coefficient due to the change of kinds of oxide debris from the rufous rust to the black one.

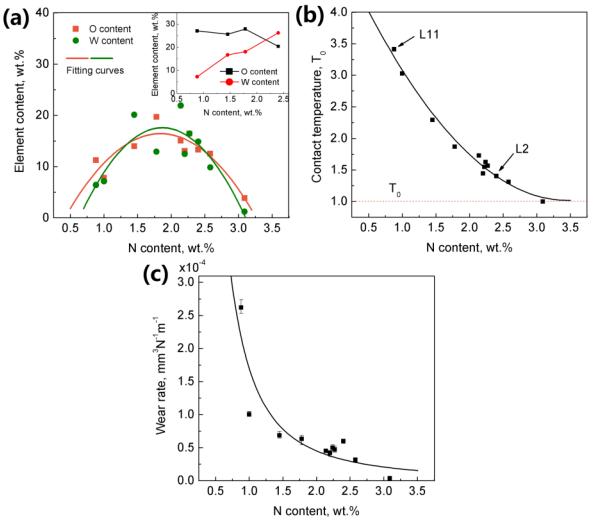

Figure 4. The EDS of O and W contents of the compacted oxide layers and wear debris

The elemental contents, especially oxygen (O) and wolfram (W), retained on the worn surface could reflect the wear mechanism. The O and W contents of the compacted oxide layers and wear debris are measured by EDS as shown in Figure 4 a. It obviously exhibits that the variations of O and W content of the compacted oxide layers approximately fit with a parabolic-law. With the decrease of the N content in the αN phase, the O and W content increases gradually, which indicates the wear mechanism shows more adhesive characters. When the N content is less than 1.5 wt.%, the O and W content drops down due to the large size of wear debris particles which would be removed out of the wear traces. The variations of the O and W content of wear debris represent an opposite tendency with the N content of expanded martensite (see inset in Fig. 4a). The O content of wear debris increases from 20.42 to 27.12 wt.% with the decrease of N content of expanded martensite from 2.4 to 0.8 wt.%. However, the corresponding W content decreases from 26.26 to 7.26 wt.%. In fact, it cannot avoid heat generation during the dry sliding process. The accumulated thermal energy would make the sliding system unstable associating with oxidation, wear debris generation and transition in wear mechanism [26]. Many studies have pointed out that the contact temperature (Tf) is considerably high enough for the generation of oxides even in the low-load and low-speed sliding conditions [18, 27, 28]. The contact temperature (Tf) depends on the friction coefficient (μ) and the hardness of wear surface (H), which can be estimated as follows [29]:

$$T_f = K\mu / H \quad \text{.....(2)}$$

Where *K* is a constant related to the normal load and the sliding speed. Figure 4b gives the ratios of contact temperature of each layer and that of the L0 layer (T_0). It is seen that the contact temperature of the L11 layer is about $3.5T_0$, which is two times higher than that of the L2 layer with value of $1.5T_0$. The elevated contact temperature of the L11 layer indeed makes the kinds of oxides changed, which results in the increase of the O content of wear debris and the decrease of the friction coefficient comparing with those of the L2 layer. The wear rates dramatically increase with N content decreasing as illustrated in Figure 4c, indicating the α_N phase has a good wear resistance because of the higher N content and hardness.

4. Conclusions

In summary, the effect of N content on the friction and wear behavior of nitrogen expanded martensite has been investigated systematically. The results of wear tests indicate that the friction and wear behavior of nitrogen expanded martensite represents a typical mild-oxidational wear mode termed an 'oxidation-scrape-reoxidation' mechanism under our present sliding condition. The variations of friction coefficient depend on competition between the compaction and delamination of oxide debris which is related to the N content and hardness of expanded martensite. The higher N contents result in the brittleness of the compacted oxide layer while the lower ones deteriorate the bearing capacity of the nitrogen expanded martensite.

The heat generation during the dry sliding process could affect the friction and wear behavior by varying the kinds of oxides (from the rufous rust to the black one) and make transition in wear mechanism. The nitrogen expanded martensite represents an excellent wear property due to the high N solution resulting in a high hardness.

Acknowledgments

This work was financially supported by the National Natural Science Foundation of China (Grant No. 51809161) and Shanghai Municipal Natural Science Foundation (Grant No.18ZR1416000).

Conflicts of Interest:

The author declares no conflict of interest.

References

1. H. Dong, “S-phase surface engineering of Fe-Cr, Co-Cr and Ni-Cr alloys”, Int. Mater. Rev, 55 65-98 (2010).
2. T. Christiansen and M. A. J. Somers, “On the crystallographic structure of S-phase”, Scripta Mater, 50, 35-37 (2004).
3. S. K. Kim, J. S. Yoo, J. M. Priest and M. P. Fewell, “Characteristics of martensitic stainless steel nitrided in a low-pressure RF plasma”, Surf. Coat. Technol, 163-164, 380-385 (2003).
4. Y. T. Xi, D. X. Liu and D. Han, “Improvement of erosion and erosion–corrosion resistance of AISI420 stainless steel by low temperature plasma nitriding”, Appl. Surf. Sci, 254, 5953-5958 (2008).
5. C. Zhang, Y. Wang, X. Chen, H. Chen, Y. Wu, Y. Wang, L. Tang, G. Cui and D. Chen, “Catalytic behavior of LaFeO3 perovskite oxide during low-pressure gas nitriding”, Appl. Surf. Sci, 506145045 (2020).
6. X. Chen, X. Bao, Y. Xiao, C. Zhang, L. Tang, L. Yao, G. Cui and Y. Yang, “Low-temperature gas nitriding of AISI 4140 steel accelerated by LaFeO3 perovskite oxide”, Appl. Surf. Sci, 466 989-999 (2019).
7. X. Wang, M. Yan, R. Liu and Y. Zhang, “Effect of rare earth addition on microstructure and corrosion behavior of plasma nitrocarburized M50NiL steel”, J. Rare Earth, 34 1148-1155 (2016).
8. Y. You, J. Yan and M. Yan, “Atomistic diffusion mechanism of rare earth carburizing/nitriding on iron based alloy”, Appl. Surf. Sci, 484, 710-715 (2019).
9. S. Karaoğlu, “Structural characterization and wear behavior of plasma-nitrided AISI 5140 low-alloy steel”, Mater. Charact, 49, 349-357 (2002).
10. Y. X. Wang, Z. B. Chen, M. F. Yan, C. S. Zhang, H. T. Chen and Y. D. Zhu, “Preparation and characterization of ultra-refined expanded martensite α’N, Surf”, Coat. Technol, 326 216-223 (2017).
11. B. Wang, S. Sun, M. Guo, G. Jin, Z. Zhou and W. Fu, “Study on pressurized gas nitriding characteristics for steel 38CrMoAlA”, Surf. Coat. Technol, 27960-64 (2015).
12. B. Wang, W. Fu, F. Dong, G. Jin, W. Feng, Z. Wang and S. Sun, “Significant acceleration of nitriding kinetics in pure iron by pressurized gas treatment”, Mater. Des, 85 91-96 (2015).
13. M. Dai, C. Li and J. Hu, “The enhancement effect and kinetics of rare earth assisted salt bath nitriding”, J. Alloy. Compd, 688 350-356 (2016).
14. A. Alsaran, “Determination of tribological properties of ion nitrided AISI 4140 steel”, Mater. Charact, 49,171-176 (2003).
15. M. F. Yan, R. L. Liu and D. L. Wu, “Improving the mechanical properties of 17-4PH stainless steel by low temperature plasma surface treatment”, Mater. Design, 31, 2270-2273 (2010).
16. M. X. Wei, S. Q. Wang, K. M. Chen and X. H. Cui, “Relations between oxidative wear and Cr content of steels”, Wear, 272, 110-121 (2011).
17. Y. P. Ji, S. J. Wu, L. J. Xu, Y. Li and S. Z. Wei, “Effect of carbon contents on dry sliding wear behavior of high vanadium high speed steel”, Wear, 294–295, 239-245 (2012).
18. F. H. Stott, “The role of oxidation in the wear of alloys”, Tribology Int, 31, 61-71 (1998).

19. C. X. Li and T. Bell, “Sliding wear properties of active screen plasma nitrided 316 austenitic stainless steel”, Wear, 256, 1144-1152 (2004).

20. G. Li, Q. Peng, Y. Wang, J. Gao, S. Chen, J. Wang and B. Shen, “Effect of DC plasma nitriding temperature on microstructure and dry-sliding wear properties of 316L stainless steel”, Surf. Coat. Technol, 202, 2749–2754 (2008).

21. M. Heydarzadeh Sohi, M. Ebrahimi, A. Honarbakhsh Raouf and F. Mahboubi, “Effect of plasma nitriding temperature on the corrosion behavior of AISI 4140 steel before and after oxidation”, Surf. Coat. Technol, 205, S84-S89 (2010).

22. H. Goto and Y. Amamoto, “Improvement of wear resistance for carbon steel under unlubricated sliding and variable loading conditions”, Wear, 270, 725-736(2011).

23. S. Lathabai, “An SEM study of mild-to-severe wear transition in grey cast iron during dry sliding”, Scripta Mater, 38, 1557-1562 (1998).

24. X. H. Cui, S. Q. Wang, F. Wang and K. M. Chen, “Research on oxidation wear mechanism of the cast steels”, Wear, 265, 468-476 (2008).

25. J. R. Jiang, F. H. Stott and M. M. Stack, “A mathematical model for sliding wear of metals at elevated temperatures”, Wear, 181-183, 20-31 (1995).

26. H. A. Abdel-Aal, “On the interdependence between kinetics of friction-released thermal energy and the transition in wear mechanisms during sliding of metallic pairs”, Wear, 254, 884-900 (2003).

27. H. So, “The mechanism of oxidational wear”, Wear, 184, 161-167 (1995).

28. M. Kalin, “Influence of flash temperatures on the tribological behaviour in low-speed sliding: A review”, Mater. Sci. Eng. A, 374, 390-397 (2004).

29. M. Z. Huq and J.P. Celis, “Expressing wear rate in sliding contacts based on dissipated energy”, Wear, 252, 375-383 (2002).

Citation: Yunxia Chen et al. “Study on friction and wear behavior of nitrogen expanded martensite under low-load and low-speed sliding condition”. SVOA Materials Science &Technology 2:3(2020) 51-57.